INSTITUTE OF PHYSICS PUBLISHING PLASMA SOURCES SCIENCE AND TECHNOLOGY

Plasma Sources Sci. Technol. **14** (2005) 152–167 doi:10.1088/0963-0252/14/1/017

Two-dimensional equilibrium of a low temperature magnetized plasma

A Fruchtman, G Makrinich and J Ashkenazy[1]

Holon Academic Institute of Technology, 52 Golomb St., Holon 58102, Israel

Received 30 June 2004
Published 1 February 2005
Online at stacks.iop.org/PSST/14/152

Abstract

A two-dimensional steady-state model is developed, in which, even though ion inertia is retained, a variable separation allows us to analyse separately the axial and the radial transports. For the axial transport (along magnetic field lines) an integral dispersion relation is derived that includes a nonlinear form that is obtained from the ion–neutral collision operator. The dispersion relation is solved for various values of the Paschen parameter, and the electron temperature and the axial profiles of the plasma density and plasma potential are calculated. The solutions of the dispersion relation are shown to have three asymptotic limits: collisionless, linear diffusion and nonlinear diffusion. For the radial transport, the rate of which is determined by electron cross-field diffusion, the full equations are numerically solved. The calculations are compared to probe measurements performed at various locations inside our helicon source for various magnetic field intensities and wave powers. The proposition that the measured increase in the plasma density with the increase of the magnetic field intensity is a result of an improved confinement, is examined. For the parameters of the experiment described here, this proposition implies that the electron collisionality is much larger than expected from electron–ion and electron–neutral collisions. A different explanation for the dependence of the density on the magnetic field intensity is suggested, that the density increase that follows an increase of the magnetic field intensity results from an improved wave–plasma coupling via the helicon interaction, causing a larger fraction of the total wave power to be deposited inside the helicon source.

1. Introduction

Considerations of particle and energy balance are often used to estimate the electron temperature and density in low temperature plasmas. In models that describe the steady-state in such plasmas, particle balance usually determines the electron temperature, while energy balance determines the plasma density [1]. In order to quantitatively estimate the balance between volume ionization and transport through the boundaries, the spatial distributions of the plasma variables should be found by a solution of the appropriate fluid equations. In this paper we present a theoretical model that improves the calculation of particle and energy balance in low temperature plasmas as well as of the spatial distributions of the plasma parameters. We then employ the model to analyse the measurements in our helicon plasma source.

The model we develop concerns the common configuration of a finite length azimuthally symmetric plasma cylinder that is immersed in an axial magnetic field. The fluid equations that describe the plasma are two dimensional. The transformation of these partial differential equations into two sets of ordinary differential equations for the radial and for the axial directions, as a result of a variable separation, provides a convenient tool for the calculation of the distributions of the plasma variables. Usually the variable separation technique is used within the diffusion approximation. The first new aspect of our model is the extension of the use of a variable separation beyond the diffusion approximation also to cases in which ion inertia is retained. That way we can analyse the two-dimensional equilibrium by solving two separate sets of

[1] While on Sabbatical from Propulsion Physics Laboratory, Soreq NRC, Yavne 81800, Israel.

ordinary differential equations for the axial and for the radial directions not only in the collisional regime but also in the collisionless regime (in which the ion inertia is dominant). The two sets of equations are decoupled except for two parameters (one of them the electron temperature) which are present in both sets. Upon imposing boundary conditions, the two parameters turn into eigenvalues of the problem. The governing fluid equations and the separation of variables are presented in section 2.

Ion–neutral collisions usually determine the plasma confinement along magnetic field lines. The second new aspect in this paper is the formulation of a model for these collisions that has an extended regime of validity. Godyak [2] has derived an expression for the drag the ions experience due to their charge-exchange collisions with neutrals. He has shown that, as a result of these collisions, the ion dynamics is governed by a nonlinear diffusion equation, which he later generalized to include the effect of ion inertia [3]. Recently, Breizman and Arefiev [4] have performed a kinetic analysis of the ion dynamics, in which, by employing self-consistent perturbative methods, they calculated the nonlinear drag on the ions. In those treatments of the ion–neutral collisions the neutral motion was neglected and the neutrals were therefore considered an immobile background. When the ion velocity is larger than the neutral velocity the neglect of the neutral velocity is reasonable, since the relative ion–neutral velocity approximately equals the ion velocity. However, when the ion flow velocity is small, the relative ion–neutral velocity is on the order of the neutral thermal velocity that should not, therefore, be neglected. In particular, for a high gas pressure the ion flow velocity is small in most of the plasma volume and the neglect of the neutral thermal velocity is not justified. Indeed, the limit on the validity of the nonlinear drag model, in which the neutral thermal velocity is zero, has been pointed out by Godyak [3]. The regime of validity of our model is extended, since we include in the collision operator collisions between ions and neutrals of a finite-temperature Maxwellian distribution. In our so-generalized model we do not, however, self-consistently solve for the ion distribution function, as was done in [4] for the immobile-neutrals case, but we rather assume a cold-beam ion distribution function. With this simplifying assumption we are able to integrate the collision operator and to derive an approximated general form for the drag force between ions and neutrals, a form that retains the nonlinear drag as well as the effect of the neutral motion for low ion velocities. At the limit of high gas pressure (in many cases around 10 mTorr, see section 4) the general form of drag force on the ions derived here ends up being linear in their velocity, correctly resulting in the familiar linear diffusion, that has been excluded from the previous models [2,4]. At intermediate pressures the nonlinear diffusion [2,4] is recovered, and, when the pressure is low, ion–neutral collisions become negligible altogether. The analysis of the collision operator and the derivation of the generalized form of the drag force are performed in appendix A.

In section 3 we employ the generalized form of the drag force between ions and neutrals, derived in appendix A, to solve the plasma dynamics along magnetic field lines. We make an approximation that allows us to employ the variable separation that we introduced in section 2 and to analyse separately the dynamics in the axial direction. We identify three distinct regimes in which the ion dynamics takes three different forms. Not surprisingly, the form that the ion dynamics along the magnetic field lines takes is determined by the value of a dimensionless parameter that is proportional to the product of the gas pressure and the plasma length (as is the Paschen parameter), or, equivalently, to the number of ion mean free paths along the system (the Knudsen number). When this dimensionless parameter is small, the ions are collisionless. At larger values of this parameter the nonlinear ion diffusion is dominant, while at even larger values linear diffusion governs the plasma dynamics. We determine the values of the Paschen parameter at the transitions between the various regimes, and derive the asymptotic values of various physical quantities.

In appendix B we apply the equations of section 2 for the case that the ion inertia is neglected in both radial and axial directions and derive two decoupled diffusion equations in the two directions. The diffusion equation along the magnetic field lines is equivalent to the equations derived in section 3 and in the appropriate limits is reduced to either the standard linear diffusion equation or to the nonlinear diffusion equation previously derived [2]. When the ion inertia can be neglected in the radial direction, the solution of the diffusion equation in that direction provides us with a relation between the two eigenvalues mentioned above, a relation that holds even if the ion inertia is retained in the axial direction, along field lines. This relation, which is valid when the ion inertia can be neglected in the radial direction, is used in appendix C to express in a more explicit way the various asymptotic relations derived in section 3. Numerical examples are presented in section 4. The axial steady state is calculated for various cases and the general solutions are compared to the solutions given by the asymptotic limits.

A uniform gas density and a uniform electron temperature are simplifying assumptions that we make in our model. The assumption of a uniform gas density is valid at the weak ionization regime, when the plasma only slightly affects the gas parameters. The assumption of a uniform electron temperature relies on the assumed high electron heat conduction. Both assumptions simplify the analysis and allow us to perform the variable separation that is inherent to our model. However, when we assume a uniform gas density, we ignore nonuniformities that result from neutral depletion [5, 6]. Nonuniform electron temperature could follow a nonuniformity in the gas density as well as nonuniformities in the deposition of external energy in the plasma. Indeed, the profiles of the plasma density that we deduce from probe measurements in our helicon plasma source are not symmetrical in the axial direction, indicating that at least one of the assumptions, a uniform neutral density or a uniform electron temperature, does not hold. In order to take advantage of the variable separation we apply our model to the experiment nevertheless, assuming that the experimental and theoretical average values of the temperature and the density should be similar. Although a considerable number of theoretical investigations have been carried out that addressed the spatial distribution of the wave energy deposition in the plasma [7–12] and some have also used the calculated distribution of energy deposition to calculate the nonuniform distribution of the electron temperature [13–15], there is an advantage to our simple model which allows a variable separation in solving the steady-state equations for the plasma.

The experiment and the probe measurements are described in section 5. The experimental results described here are detailed measurements of the ion saturation current into a Langmuir probe inside a helicon plasma source [16–24]. The ion saturation current was measured in various locations inside the source as a function of the applied magnetic field intensity and of the wave power. We then attempt to understand the dependence of the plasma density (deduced from the measured ion saturation current) on the magnetic field intensity and on the wave power. The dependence of the plasma density on the magnetic field intensity is often discussed in the literature, usually in relation to the helicon wave–plasma interaction. In this paper we apply our model to seek the relation between the dependence of the plasma density on the magnetic field intensity and on the wave power and particle and energy balance. There are two possible reasons for the observed increase in density with the increase of the magnetic field intensity. One such reason is an improved radial confinement by the magnetic field. We show that if the better confinement is indeed the main reason for the density increase, it is implied that the electron collisionality that causes the transport of the electrons across the magnetic field lines is much larger than expected from electron–ion and electron–neutral collisions. Although the high collisionality is also consistent with the weak dependence of the plasma impedance on the magnetic field intensity, as we indeed see experimentally, we find it hard to conclude that such a high anomalous electron collisionality actually exists in our plasma. Rather, we suggest a second reason as the main reason for the density increase. For a fixed total wave power the increase in the magnetic field increases the wave–plasma coupling via the helicon interaction, causing a larger fraction of the total wave power to be deposited inside the helicon source. This second possible reason will be examined in a following paper.

The solution of the equations in the radial direction for classical and anomalous electron resistivity and the comparison with the experiment are described in section 6. We conclude in section 7.

2. The equilibrium model

In this section we present the fluid equations that describe the steady-state of a finite length azimuthally symmetric plasma cylinder that is immersed in an axial magnetic field. We then perform a variable separation.

The plasma dynamics is governed by the continuity equation

$$\vec{\nabla}\cdot n\vec{v} = \nu_{\rm ion} n, \tag{1}$$

by the electron momentum equation, in which the electron inertia is neglected,

$$0 = en\vec{\nabla}\phi - \vec{\nabla}nT - enB\vec{v}_{\rm e} \times \vec{e}_z - nm_{\rm e}\nu_{\rm eN}\vec{v}_{\rm e} - nm_{\rm e}\nu_{\rm ei}(v_{{\rm e}\theta} - v_\theta)\vec{e}_\theta \tag{2}$$

and by the the ion momentum equation, in which the ion pressure is neglected,

$$m_{\rm i}\vec{\nabla}\cdot n\vec{v}\vec{v} = -en\vec{\nabla}\phi + enB\vec{v}\times\vec{e}_z - nm_{\rm i}\nu_{\rm iN}\vec{v} - nm_{\rm i}\nu_{\rm ie}(v_\theta - v_{{\rm e}\theta})\vec{e}_\theta. \tag{3}$$

Here B is the intensity of the applied axial magnetic field, n is the (quasineutral) plasma density, e is the elementary charge, $m_{\rm i}$ and $m_{\rm e}$ are, respectively, the ion and electron masses, $\vec{v}$ and $\vec{v}_{\rm e}$ are, respectively, the ion and electron flow velocities, $\nu_{\rm ei}$, $\nu_{\rm eN}$ and $\nu_{\rm ie} = \nu_{\rm ei}m_{\rm e}/m_{\rm i}$ are the electron–ion, electron–neutral and ion–electron collision frequencies, T is the electron temperature, ϕ is the electrostatic potential and $\nu_{\rm ion}$ is the ionization frequency. Cylindrical coordinates r, θ and z are used. The ion pressure is neglected since the ion temperature is usually smaller than the electron temperature. Adding equations (2) and (3), we obtain the momentum balance equation:

$$m_{\rm i}\vec{\nabla}\cdot n\vec{v}\vec{v} = -\vec{\nabla}nT - m_{\rm i}\vec{\vec{\nu}}n\vec{v}, \tag{4}$$

where the coefficients of the tensor $\vec{\vec{\nu}}$ are:

$$\begin{gathered}\nu_{rr} \equiv (\omega_{\rm ci}\omega_{\rm ce})/\nu_{\rm e} + \nu_{\rm iN} + (m_{\rm e}/m_{\rm i})\nu_{\rm eN},\\ \nu_{r\theta} \equiv -(\omega_{\rm ci}\nu_{\rm eN})/\nu_{\rm e},\\ \nu_{\theta\theta} \equiv (m_{\rm e}/m_{\rm i})(\nu_{\rm eN}\nu_{\rm ei})/\nu_{\rm e} + \nu_{\rm iN}, \qquad \nu_{\theta r} = -\nu_{r\theta},\\ \nu_{zz} \equiv \nu_{\rm iN} + (m_{\rm e}/m_{\rm i})\nu_{\rm eN},\\ \nu_{rz} = \nu_{\theta z} = \nu_{zr} = \nu_{z\theta} = 0.\end{gathered} \tag{5}$$

In writing equation (4) we employed the θ component of equation (2) and used the relation $v_{{\rm e}\theta} = (\omega_{\rm ce}/\nu_{\rm e})v_r + (\nu_{\rm ei}/\nu_{\rm e})v_\theta$, where $\nu_{\rm e} \equiv \nu_{\rm eN} + \nu_{\rm ei}$ and $v_{{\rm e}r} = v_r$, $v_{{\rm e}z} = v_z$. In equation (5) $\omega_{{\rm ci(e)}} \equiv eB/m_{{\rm i(e)}}$ is the ion (electron) cyclotron frequency. We analyse the case in which the plasma is surrounded by insulating walls. A conductor at the axial boundaries could enable electrons to radially cross field-lines. However, no such conductor is present, and, therefore, there is no radial or axial current in the plasma.

In a self-consistent approach, such as that of Cho and Lieberman [14], the spatial distribution of the electron temperature is determined by the spatial distribution of the wave energy deposition into the electrons and by the electron energy transport processes. We make the simplifying assumption that the electron temperature is uniform:

$$T = \text{const.} \tag{6}$$

Once this assumption is made the spatial distribution of the wave energy deposition does not affect the plasma steady-state, what matters is only the total energy deposited. The assumption of a uniform electron temperature is justified to a certain extent by the heat conductivity of the electrons being large. The implications of this assumption on the accuracy of results of the calculation will be tested in a future study. Here we take advantage of the variable separation that is made possible because of this assumption.

When the geometry, the neutral density, the intensity of the magnetic field and the transport coefficients are specified, the temperature, the electric potential and the density profile are usually determined by the solutions of equations (1) and (4) that describe particle balance, and by the requirement that the boundary conditions be satisfied. The actual value of the plasma density is determined by power balance:

$$\begin{gathered}P = \Gamma_{\rm T}\varepsilon_{\rm T}, \qquad \Gamma_{\rm T} \equiv \oint n v_\perp \,{\rm d}S = \int \nu_{\rm ion} n \,{\rm d}V,\\ \varepsilon_{\rm T} = \varepsilon_{\rm c} + 2T + 0.5T\left[1 + \ln\left(\frac{1}{2\pi}\frac{m_{\rm i}}{m_{\rm e}}\right)\right].\end{gathered} \tag{7}$$

Here P, the total deposited power, is equal to the rate of plasma generation (which equals the rate at which plasma escapes from that volume Γ_T) multiplied by ε_T, the average energy lost in the production of one electron–ion pair [1]. This lost energy includes the energy cost for ionization ε_c, and the energy lost by electrons and ions at the plasma boundaries. We note that, as long as no current is drawn at the plasma boundaries, the energy gained by the ions while crossing the sheath at these boundaries (an energy that is several times the electron temperature) is equal to the energy lost by the electrons that cross the sheath. When this energy is included in ε_T, it should be understood as an energy that has been deposited in the electrons in the plasma bulk. We also note that the total particle flux Γ_T is determined only by the total deposited power P and by the electron temperature T that determines ε_T.

We turn now to solve the equations by a variable separation. Within the assumptions of uniform transport coefficients and temperature, we seek a solution of the form:

$$\begin{aligned} &n(z,r) = n_0 f(r) g(z), \quad v_r = v_r(r), \quad v_\theta = v_\theta(r), \\ &v_{e\theta} = v_{e\theta}(r), \quad v_z = v_z(z), \quad \phi(z,r) = \phi_1(z) + \phi_2(r). \end{aligned} \tag{8}$$

The plasma column is of a length L and radius a and is assumed to be symmetrical in the z direction, so that the maximal density is at its centre, and we write $f(0) = g(0) = 1$. From the continuity and momentum equations we obtain:

$$\frac{\partial}{\partial r}(r f v_r) = \nu_r r f, \tag{9}$$

$$\nu_{ion} v_r^2 - \frac{v_r v_\theta^2}{r} + v_r^2 \frac{\partial}{\partial r} v_r = -c_s^2 \left(\nu_r - \frac{\partial}{\partial r} v_r - \frac{v_r}{r} \right) - \nu_{rr} v_r^2 + \nu_{r\theta} v_r v_\theta, \tag{10}$$

$$\nu_{ion} v_\theta + \frac{v_\theta v_r}{r} + v_r \frac{\partial}{\partial r} v_\theta = -\nu_{\theta\theta} v_\theta - \nu_{\theta r} v_r, \tag{11}$$

$$\frac{\partial}{\partial z}(g v_z) = (\nu_{ion} - \nu_r) g \tag{12}$$

and

$$\nu_{ion} v_z^2 + v_z^2 \frac{\partial}{\partial z} v_z = c_s^2 \left[\frac{\partial}{\partial z} v_z - (\nu_{ion} - \nu_r) \right] - \nu_{zz} v_z^2. \tag{13}$$

Here $c_s \equiv \sqrt{T/m_i}$ is the ion acoustic velocity. We write the ionization frequency as

$$\nu_{ion} = \beta N, \qquad \beta \equiv \langle \sigma_{ion} \boldsymbol{v}_{edf} \rangle, \tag{14}$$

where the brackets $\langle\ \rangle$ denote averaging over the electron velocity distribution function, σ_{ion} is the ionization cross section, $\boldsymbol{v}_{edf}$ is the electron velocity and N is the neutral density.

We therefore have a set of ordinary equations for the five unknown functions f, g, v_r, v_θ and v_z. The boundary conditions at the radial and axial boundaries determine the values of the parameters T and ν_r (a parameter that results from the variable separation), which turn out to be eigenvalues of the problem. Once these five functions and two parameters are found, the electron momentum equation is used to determine the values of $v_{e\theta}$, ϕ_1 and ϕ_2:

$$v_{e\theta} = \frac{\omega_{ce}}{\nu_e} v_r + \frac{\nu_{ei}}{\nu_e} v_\theta, \tag{15}$$

$$\frac{\partial \phi_1}{\partial z} = \frac{T}{e} \frac{\partial \ln g}{\partial z} + \frac{m_e \nu_{eN}}{e} v_z \tag{16}$$

and

$$\frac{\partial \phi_2}{\partial r} = \frac{T}{e} \frac{\partial \ln f}{\partial r} + B v_{e\theta} + \frac{m_e \nu_{eN}}{e} v_r. \tag{17}$$

Before continuing we note that the approximated electric potential is given by the r component of equation (3) in which we neglect the ion inertia and assume $v_\theta = 0$: $\partial\phi_2/\partial r = -(m_i \nu_{iN}/e) v_r$. Comparing this expression to equation (17) it is clear that

$$\frac{T}{e} \frac{\partial \ln f}{\partial r} \simeq -B v_{e\theta}, \qquad \frac{\partial \phi_2}{\partial r} \ll \frac{T}{e} \frac{\partial \ln f}{\partial r}. \tag{18}$$

To lowest order there is a balance in the r direction between the electron and the magnetic field pressures. The *radial* electric field is small (except very near the radial boundary where the ion inertia plays a role). The *axial* electric field, however, is not small. This results from the second term on the RHS of equation (16) being small. Neglecting this small term we obtain

$$\phi_1 \cong \frac{T}{e} \ln g. \tag{19}$$

Here the zero of the potential is at the peak potential of the plasma.

The total radial and axial fluxes through the boundaries become, when variables are separated,

$$\begin{aligned} &\Gamma_{rT} = 2\pi a L n_0 \bar{g} (f v_r)_{r=a}, \qquad \Gamma_{zT} = 2\pi a^2 n_0 \bar{f} (g v_z)_{z=L/2}, \\ &\bar{g} \equiv \frac{1}{L} \int_{-L/2}^{L/2} g(z)\, dz, \qquad \bar{f} \equiv \frac{2}{a^2} \int_0^a r f(r)\, dr \end{aligned} \tag{20}$$

and since ν_{ion} is constant across the discharge (T and N are uniform), we obtain from equations (9) and (12):

$$(r f v_r)_{r=a} = \frac{\nu_r \bar{f} a^2}{2}, \qquad (g v_z)_{z=L/2} = (\nu_{ion} - \nu_r) \bar{g} \frac{L}{2}, \tag{21}$$

so that

$$\begin{aligned} &\Gamma_{rT} = n_0 \bar{f} \bar{g} V \nu_r, \qquad \Gamma_{zT} = n_0 \bar{f} \bar{g} V (\nu_{ion} - \nu_r) \\ &\Rightarrow \Gamma_T = \Gamma_{rT} + \Gamma_{zT} = n_0 \bar{f} \bar{g} V \nu_{ion}, \end{aligned} \tag{22}$$

where $V = \pi a^2 L$ is the plasma volume. We make the (not necessarily true) assumption that $g(z) = g(-z)$.

We turn to the transport coefficient $\nu_{zz} = \nu_{iN} + (m_e/m_i)\nu_{eN} \cong \nu_{iN}$, found through the calculation of the drag on the ions due to their collisions with neutrals. The details of the calculation and the conditions for its validity are presented in appendix A. The drag force turns out to be

$$\begin{aligned} &\vec{F} = -m_i \vec{v} \left(\frac{2T_g}{m_i} \right)^{1/2} N n \sigma_{iN} \left[\left(d + \frac{1}{d} - \frac{1}{4d^3} \right) \mathrm{erf}(d) \right. \\ &\left. \quad + \frac{1}{\sqrt{\pi}} \left(1 + \frac{1}{2d^2} \right) \exp(-d^2) \right], \\ &\sigma_{iN} \equiv \sigma_{cx} + \frac{\sigma_{el}}{2}, \quad \vec{d} \equiv \left(\frac{m_i}{2T_g} \right)^{1/2} \vec{v}. \end{aligned} \tag{23}$$

Here T_g is the neutral gas temperature and σ_{cx} and σ_{el} are the cross sections for charge exchange and elastic collisions. At the limits of small and large d, the force becomes

$$\begin{aligned} &\vec{F} \cong -\tfrac{4}{3} m_i n \sigma_{iN} N v_T \vec{v}, \qquad d \ll 1, \\ &\vec{F} \cong -m_i n \sigma_{iN} N |\vec{v}| \vec{v}, \qquad d \gg 1. \end{aligned} \tag{24}$$

Here $v_T = \sqrt{8T_g/(\pi m_i)}$ is the gas thermal velocity.

The force between ions and neutrals depends on the magnitude of the ion velocity. Therefore, when the component of this force is taken along the magnetic field, the variable separation is not possible. In order to enable the variable separation we approximate the dimensionless velocity d in equation (23) by d_z. By sacrificing some accuracy, we can reduce the equations to a one-dimensional form, while the nonlinearity in the ion–neutral collisions is essentially preserved. The ion–neutral collision frequency takes the nonlinear form in the axial direction. In the radial direction, where it is less important, we keep the linear term only and use $\nu_{\mathrm{iN}} = \frac{4}{3}\sigma_{\mathrm{iN}} N v_{\mathrm{T}}$ in ν_{rr} and $\nu_{\theta\theta}$. This approximation is good near the plasma axis (where the plasma density is high) and is less accurate near the radial boundaries (where the plasma density is low). Also, when the plasma is magnetized the radial ion velocity is small except near the radial boundaries, which makes the approximation more accurate.

In the next section we employ the generalized form of the drag force between ions and neutrals derived here (equation (23)), to solve the plasma dynamics along magnetic field lines. We then derive expressions for various physical quantities at three asymptotic limits.

3. The axial flux along magnetic field lines

When we use the form of the axial force as in equation (23), equation (13) and the boundary conditions become (in dimensionless forms)

$$(1 - M_z^2)\frac{\partial M_z}{\partial \zeta} = b_{\mathrm{P}}(b_0 + b_2 M_z^2 + M_z^3) \tag{25}$$

and

$$M_z(\zeta = 0) = 0, \qquad M_z(\zeta = 1) = 1, \tag{26}$$

where the axial Mach number, dimensionless coordinate and parameters are

$$\begin{gathered} M_z \equiv \frac{v_z}{c_{\mathrm{s}}}, \qquad \zeta \equiv \frac{z}{L/2}, \qquad b_{\mathrm{P}} \equiv \frac{\sigma_{\mathrm{iN}} N L}{2}, \\ b_0 \equiv \frac{\beta}{\sigma_{\mathrm{iN}} c_{\mathrm{s}}} - \frac{\nu_r}{\sigma_{\mathrm{iN}} c_{\mathrm{s}} N}, \qquad b_2 \equiv \frac{\beta}{\sigma_{\mathrm{iN}} c_{\mathrm{s}}} + \frac{4 v_{\mathrm{T}}}{3 c_{\mathrm{s}}} P(d). \end{gathered} \tag{27}$$

The ratio $v_{\mathrm{T}}/c_{\mathrm{s}}$ is

$$\frac{v_{\mathrm{T}}}{c_{\mathrm{s}}} = \sqrt{\frac{8 T_{\mathrm{g}}}{\pi T}} \tag{28}$$

and

$$P(d) \equiv \frac{3\sqrt{\pi}}{8} d \left\{ \left[\left(1 + \frac{1}{d^2} - \frac{1}{4d^4}\right) \mathrm{erf}(d) + \frac{1}{\sqrt{\pi}} \left(\frac{1}{d} + \frac{1}{2d^3}\right) \exp(-d^2) \right] - 1 \right\}. \tag{29}$$

The variable d, defined in equation (23), can be written as a function of the Mach number M_z and the ratio $v_{\mathrm{T}}/c_{\mathrm{s}}$ as

$$d = \frac{2}{\sqrt{\pi}} \frac{c_{\mathrm{s}}}{v_{\mathrm{T}}} M_z. \tag{30}$$

The function $P(d)$ is monotonically decreasing, $P(0) = 1$ and $P(d) \longrightarrow 3\sqrt{\pi}/(8d)$ when $d \longrightarrow \infty$. The dimensionless Paschen parameter b_{P}, $b_{\mathrm{P}} = [\sigma_{\mathrm{iN}}/(2T_{\mathrm{g}})] P_{\mathrm{g}} L$, is proportional to the product of the gas pressure P_{g} and the system length $L/2$. It is also inversely proportional to the Knudsen number, which is proportional to the ratio of the ion mean free path, $\lambda_{\mathrm{i}} \equiv (\sigma_{\mathrm{iN}} N)^{-1}$, to the system length. Note also that b_2 is not constant but rather varies with M_z.

To the momentum equation we add the dimensionless continuity equation:

$$\frac{\partial (g M_z)}{\partial \zeta} = b_{\mathrm{P}} b_0 g \quad \Longrightarrow \quad g_{\mathrm{s}} = b_{\mathrm{P}} b_0 \bar{g}, \tag{31}$$

which is integrated with the aid of equation (25) to calculate g_{s}, the value of g at the sheath at the axial boundaries.

The momentum equation, equation (25), is integrated to give a relation between M_z and ζ. When the boundary conditions, equation (26), are imposed, a dispersion relation is obtained, which provides us with a relation between ν_r and T, in addition to the relation between these two parameters that we obtain from the radial equations. The relation between M_z and ζ and the dispersion relation are:

$$\begin{gathered} \int_0^{M_z} \frac{(1 - M_z'^2)}{(b_0 + b_2 M_z'^2 + M_z'^3)} \, \mathrm{d}M_z' = b_{\mathrm{P}} \zeta, \\ \int_0^1 \frac{(1 - M_z^2)}{(b_0 + b_2 M_z^2 + M_z^3)} \, \mathrm{d}M_z = b_{\mathrm{P}}. \end{gathered} \tag{32}$$

Combining equations (25) and (31) we obtain the relations

$$\begin{gathered} g = \exp\left\{ - \int_0^{M_z} \frac{[(b_0 + b_2)x + x^2]}{(b_0 + b_2 x^2 + x^3)} \, \mathrm{d}x \right\}, \\ g_{\mathrm{s}} = \exp\left\{ - \int_0^1 \frac{[(b_0 + b_2)x + x^2]}{(b_0 + b_2 x^2 + x^3)} \, \mathrm{d}x \right\}. \end{gathered} \tag{33}$$

Following these relations, equation (19) yields

$$\begin{gathered} \phi = -\frac{T}{e} \int_0^{M_z} \frac{[(b_0 + b_2)x + x^2]}{(b_0 + b_2 x^2 + x^3)} \, \mathrm{d}x, \\ \phi_{\mathrm{s}} = -\frac{T}{e} \int_0^1 \frac{[(b_0 + b_2)x + x^2]}{(b_0 + b_2 x^2 + x^3)} \, \mathrm{d}x. \end{gathered} \tag{34}$$

We turn now to derive expressions for M_z, g and ϕ in several limits. We discuss three cases. One case is of linear diffusion. In this case the collision operator is linear and the third term in both denominators of equation (32) is neglected. A second case is that of nonlinear diffusion, in which the collision operator is nonlinear and the second term in both denominators of equation (32) is neglected. In both linear and nonlinear diffusion cases the ion inertia, the second term in the numerators of equation (32), is neglected. In the third case the ion inertia, represented by the second term in both numerators of the equations, is retained, while the third term in the denominators is neglected.

We first determine the transition between the case that the collision operator is linear to the case that it is nonlinear. Both the second and third terms in the denominator of the integrand are monotonically increasing functions of M_z. The transition between the dominance of the second term and the third term occurs at $M_z = M_{z,t}$ that satisfies the equality

$$M_{z,t} = b_2(M_{z,t}). \tag{35}$$

The second term is dominant for $M_z \ll M_{z,t}$ while the third term is dominant for $M_z \gg M_{z,t}$. The third term in the denominator can be neglected if

$$M_{z,t}^3 \gg b_0, \tag{36}$$

because the integrand is then small for $M \gg M_{z,t}$. In this case the collision operator is linear. The second term in the denominator can be neglected if

$$M_{z,t}^3 \ll b_0 \tag{37}$$

and the collision operator is nonlinear. Equivalently to equations (36) and (37) we write the conditions for the two cases in the following forms. The collision operator is linear when

$$b_0^{1/3} \ll M_{z,t} = b_2(M_{z,t}) \ll b_2(b_0^{1/3}) = \frac{\beta}{\sigma_{\rm iN} c_{\rm s}} + \frac{4 v_{\rm T}}{3 c_{\rm s}} P\left(\frac{2}{\sqrt{\pi}} \frac{c_{\rm s}}{v_{\rm T}} b_0^{1/3}\right) \tag{38}$$

and is nonlinear when

$$b_0^{1/3} \gg b_2(b_0^{1/3}). \tag{39}$$

Note that b_2 is a decreasing function of M_z.

3.1. The collision operator being linear

Let us discuss the form of $b_2(b_0^{1/3})$ in the case that the collision operator is linear. When

$$\frac{2}{\sqrt{\pi}} \frac{c_{\rm s}}{v_{\rm T}} b_0^{1/3} \ll 1, \tag{40}$$

the condition for the collision operator to be linear (38) becomes

$$b_0^{1/3} \ll \frac{\beta}{\sigma_{\rm iN} c_{\rm s}} + \frac{4 v_{\rm T}}{3 c_{\rm s}}, \tag{41}$$

while when

$$\frac{2}{\sqrt{\pi}} \frac{c_{\rm s}}{v_{\rm T}} b_0^{1/3} \gg 1, \tag{42}$$

the condition becomes:

$$b_0^{1/3} \ll \frac{\beta}{\sigma_{\rm iN} c_{\rm s}} + \frac{\pi}{4 b_0^{1/3}} \left(\frac{v_{\rm T}}{c_{\rm s}}\right)^2. \tag{43}$$

This can happen only if

$$\frac{\beta}{\sigma_{\rm iN} c_{\rm s}} \gg \frac{\pi}{4 b_0^{1/3}} \left(\frac{v_{\rm T}}{c_{\rm s}}\right)^2. \tag{44}$$

Otherwise

$$b_0^{1/3} \ll \frac{\pi}{4 b_0^{1/3}} \left(\frac{v_{\rm T}}{c_{\rm s}}\right)^2, \tag{45}$$

which contradicts our assumption, equation (42). If indeed equation (44) holds, we can neglect the second term in the expression for b_2 altogether. It turns out, therefore, that when the collision operator is linear we can safely write

$$b_2 = \frac{\beta}{\sigma_{\rm iN} c_{\rm s}} + \frac{4 v_{\rm T}}{3 c_{\rm s}}. \tag{46}$$

Since b_2 in this form is constant and independent of M_z, we integrate equation (32), in which we neglect the third term in both denominators, and equation (31). As a result we obtain

$$b_{\rm P} b_2 \zeta = -M_z + \left(\frac{1}{s} + s\right) \arctan(s M_z),$$
$$g = \left(\frac{1}{1 + s^2 M_z^2}\right)^{(1/2)(1+(1/s^2))},$$
$$g_{\rm s} = \left(\frac{1}{1 + s^2}\right)^{(1/2)(1+(1/s^2))}, \qquad s \equiv \left(\frac{b_2}{b_0}\right)^{1/2}. \tag{47}$$

The dispersion relation becomes

$$b_{\rm P} b_2 = -1 + \left(\frac{1}{s} + s\right) \arctan(s). \tag{48}$$

3.2. Linear diffusion

When the collision operator is linear, the ion inertia can be neglected if

$$b_0 \ll b_2. \tag{49}$$

Neglecting the ion inertia, the second term in both numerators of equation (32), we obtain

$$M_z = \left(\frac{b_0}{b_2}\right)^{1/2} \tan[b_{\rm P} (b_0 b_2)^{1/2} \zeta],$$
$$g = \sqrt{\frac{1}{1 + (b_2/b_0) M_z^2}} = \cos[b_{\rm P} (b_0 b_2)^{1/2} \zeta], \tag{50}$$

$$g_{\rm s} = \left(\frac{b_0}{b_2}\right)^{1/2}, \qquad \bar{g} = \frac{2}{\pi} = 0.636\,62 \tag{51}$$

and the approximate dispersion relation in the form:

$$b_{\rm P} (b_0 b_2)^{1/2} = \frac{\pi}{2}. \tag{52}$$

This is the linear diffusion result. Note that sometimes the ion inertia can be neglected even in the collisionless case, in which $b_{\rm P} = 0$. That happens when ionization is balanced by radial diffusion $\beta \approx v_r/N$, so that $b_0 \ll b_2$.

The requirements for the validity of the linear diffusion case, as formulated above, $b_0 \ll b_2$ and $b_0^{1/3} \ll b_2$, together with equation (52), result in

$$b_{\rm P} b_2 \gg \frac{\pi}{2} \qquad \text{and} \qquad b_{\rm P} b_2^2 \gg \frac{\pi}{2}, \tag{53}$$

respectively. Since $b_0 \ll b_2$ we can approximate

$$b_2 \cong b_2 - b_0 = \frac{\nu_r L}{2 c_{\rm s} b_{\rm p}} + \frac{4 v_{\rm T}}{3 c_{\rm s}}. \tag{54}$$

Equations (53) and (54) are now written in a form that determines the regime of validity of the linear diffusion case as

$$\frac{\nu_r L}{2 c_{\rm s}} + \frac{4 v_{\rm T}}{3 c_{\rm s}} b_{\rm p} \gg \frac{\pi}{2}, \quad \sqrt{\frac{\pi}{2}} b_{\rm P}. \tag{55}$$

When the conditions (55) hold, the solution of the dispersion relation (52) and $g_{\rm s}$ become

$$\frac{\beta N L}{2 c_{\rm s}} = \frac{\nu_r L}{2 c_{\rm s}} + \left(\frac{\pi}{2}\right)^2 \left(\frac{\nu_r L}{2 c_{\rm s}} + \frac{4 v_{\rm T}}{3 c_{\rm s}} b_{\rm p}\right)^{-1},$$
$$g_{\rm s} = \left(\frac{b_0}{b_2}\right)^{1/2} = \frac{\pi}{2} \left(\frac{\nu_r L}{2 c_{\rm s}} + \frac{4 v_{\rm T}}{3 c_{\rm s}} b_{\rm p}\right)^{-1}. \tag{56}$$

The ionization is balanced by radial transport and axial linear diffusion.

3.3. Retaining the ion inertia

When the collision operator is linear, the ion inertia should be retained when $b_0 \cong b_2$. This happens when both radial transport and collisions are small

$$b_0 \cong b_2 = \frac{\beta}{\sigma_{\rm iN} c_{\rm s}}, \qquad \frac{\beta N L}{2c_{\rm s}} \gg \frac{\nu_r L}{2c_{\rm s}}, \quad \frac{4v_{\rm T}}{3c_{\rm s}} b_{\rm p}. \tag{57}$$

When these conditions are combined with the condition for the collision operator being linear, $b_0^{1/3} \ll b_2 \cong b_0$, we find that $b_0 = \beta/(\sigma_{\rm iN} c_{\rm s})$ is much larger than unity. In that case

$$\left(\frac{\pi}{2} - 1\right)\zeta = -M_z + 2\arctan(M_z), \qquad g = \frac{1}{1+M_z^2},$$
$$g_{\rm s} = \frac{1}{2}, \qquad \bar{g} = \frac{0.5}{\pi/2 - 1} = 0.875\,97 \tag{58}$$

and the dispersion relation becomes

$$b_{\rm P} b_0 = \frac{\beta N L}{2c_{\rm s}} = \frac{\pi}{2} - 1. \tag{59}$$

Since $b_2 = b_0 \gg 1$ it means that $b_{\rm P} \ll 1$. This is the fluid description of the free-fall presheath that is usually described kinetically [25]. The ion inertia case is therefore retained when

$$\frac{\beta N L}{2c_{\rm s}} = \frac{\pi}{2} - 1 \gg \frac{\nu_r L}{2c_{\rm s}}, \qquad 1 \gg b_{\rm p}. \tag{60}$$

In summary, if $b_{\rm P} \ll 1$ and $\nu_r L/(2c_{\rm s}) \ll \pi/2 - 1$, we obtain the solution (59), valid for the small radial transport, collisionless case.

3.4. The nonlinear diffusion

When the collision operator is nonlinear, the ion inertia can be neglected if

$$b_0 \ll 1. \tag{61}$$

Since $b_0 \leqslant b_2$, the condition for the collision operator being nonlinear, $b_0^{1/3} \gg b_2$, holds only if $b_0^{1/3} \gg b_0$, resulting in $b_0 \ll 1$. Therefore, inequality (61) always holds, and the ion inertia can always be neglected, when the collision operator is nonlinear. In summary, the conditions for the validity of the collision operator being nonlinear are

$$b_2 = \left(\frac{\beta}{\sigma_{\rm iN} c_{\rm s}} + \frac{4v_{\rm T}}{3c_{\rm s}} P\right) \ll b_0^{1/3}$$
$$= \left(\frac{\beta}{\sigma_{\rm iN} c_{\rm s}} - \frac{\nu_r}{\sigma_{\rm iN} c_{\rm s} N}\right)^{1/3} \ll 1. \tag{62}$$

The left inequality ensures the nonlinear diffusion, while the right inequality justifies the neglect of the ion inertia. As we explained above, the left inequality insures the right inequality, which means that when the nonlinear diffusion is valid, the ion inertia can be neglected.

This regime, in which the nonlinear collision term is dominant, was explored by Godyak [2]. The solution of equation (32), when the second term in the denominator and the ion inertia are neglected, becomes

$$b_{\rm P} b_0^{2/3} \zeta = \int_0^{M_z/b_0^{1/3}} \frac{{\rm d}x}{1+x^3}, \qquad g = \frac{1}{(1 + M_z^3/b_0)^{1/3}}. \tag{63}$$

In order to obtain the expression for the density we used the simplified nonlinear form of equation (25), in which the ion inertia was neglected, and equation (31). Consistently with the neglect of the ion inertia we assume that M_z is infinite at $\zeta = 1$ and obtain the following approximate expressions and dispersion relation:

$$b_{\rm P} b_0^{2/3} = \alpha_{\rm G}^{2/3} \equiv \int_0^\infty \frac{{\rm d}x}{1+x^3} = \frac{2\pi}{3\sqrt{3}},$$
$$g_{\rm s} = \frac{\alpha_{\rm G}^{1/3}}{b_{\rm P}^{1/2}}, \qquad \bar{g} = \frac{1}{\alpha_{\rm G}^{2/3}}. \tag{64}$$

We note that $(g v_z)_{\rm s}$ approximately equals $b_0^{1/3} c_{\rm s}$ and, as expected from a diffusion approximation, is independent of the exact value of the ion velocity at the plasma edge. The solution of the dispersion relation can also be written as

$$\frac{\beta N L}{2c_{\rm s}} = \frac{\nu_r L}{2c_{\rm s}} + \frac{\alpha_{\rm G}}{b_{\rm P}^{1/2}}. \tag{65}$$

The ionization is balanced by radial transport and axial nonlinear diffusion.

We use equation (65) in order to express b_2 as $b_2 = \nu_r L/(2c_{\rm s} b_{\rm P}) + \alpha_{\rm G}/b_{\rm P}^{3/2} + [4\nu_{\rm T}/(3c_{\rm s})]P[2c_{\rm s}\alpha_{\rm G}^{1/3}/(\sqrt{\pi}\nu_{\rm T} b_{\rm p}^{1/2})]$. Inequalities (62) and the resulting dispersion relation (64) together define the regime of validity of this approximation as $\alpha_{\rm G}^{2/3} \ll b_{\rm P} \ll \alpha_{\rm G}^{2/3}(b_2)^{-2}$. The right inequality can be written as $b_2 \ll \alpha_{\rm G}^{1/3}/b_{\rm P}^{1/2}$. Therefore, $\alpha_{\rm G}^{1/3}/b_{\rm P}^{1/2}$ has to be much larger than each of the three terms composing b_2. It can be easily verified that, in order to be larger than the third term in the expression for b_2, the argument of P should be much larger than unity. The requirements for validity of the nonlinear approximation become

$$\left(\frac{\nu_r L}{2c_{\rm s}}\right)^2 \frac{1}{\alpha_{\rm G}^{2/3}}, \alpha_{\rm G}^{2/3} \ll b_{\rm P} \ll \frac{4\alpha_{\rm G}^{2/3}}{\pi}\left(\frac{c_{\rm s}}{v_{\rm T}}\right)^2. \tag{66}$$

We have therefore characterized the three asymptotic regimes for the ion axial transport, the linear diffusion, the nonlinear diffusion and the ion inertia regime.

In appendix B we reexamine the diffusion regime, which encompasses both linear and nonlinear diffusions in the axial direction, and a linear diffusion in the radial direction. This diffusion regime is obtained when we make the approximations of neglecting the ion inertia in both axial and radial directions as well as the azimuthal ion velocity, so that $v_\theta = 0$. As is shown in appendix B, the linear diffusion in the radial direction yields the well-known form for the parameter ν_r,

$$\nu_{rr} = \frac{\omega_{\rm ci}\omega_{\rm ce}}{\nu_{\rm e}},$$
$$\nu_r = \frac{p_1^2}{a^2}\frac{c_{\rm s}^2}{\nu_{rr}} = \frac{p_1^2}{a^2}\frac{c_{\rm s}^2 \nu_{\rm e}}{\omega_{\rm ci}\omega_{\rm ce}}, \quad p_1 = 2.4048. \tag{67}$$

In appendix C we rewrite the asymptotic expressions derived in this section for the case the linear diffusion holds in the

radial direction and the parameter ν_r takes the form as in equation (67).

In the next section we demonstrate the three asymptotic limits within a numerical example.

4. Numerical example

Let us assume that the plasma is strongly magnetized,

$$\nu_r = 0, \tag{68}$$

so that the radial diffusion is negligible. We then neglect the terms proportional to ν_r (or to $\nu_e/\omega_{ci}\omega_{ce}$) in the equations. Employing the relations from the previous section, the three regimes, the ion inertia regime (60), the nonlinear diffusion regime (66), and the linear diffusion regime (55), are reduced to

$$\begin{gathered}(1)\quad b_P \ll 1, \qquad (2)\quad \alpha_G^{2/3} \ll b_P \ll \frac{4\alpha_G^{2/3}}{\pi}\left(\frac{c_s}{v_T}\right)^2, \\ (3)\quad b_p \gg \frac{9\pi}{32}\left(\frac{c_s}{v_T}\right)^2.\end{gathered} \tag{69}$$

Using the form $b_P = [\sigma_{iN}/(2T_g)]P_gL$, we find that the transition between the nonlinear and linear diffusion occurs when the Paschen parameter has the approximate value

$$P_gL \approx \frac{T}{\sigma_{iN}}. \tag{70}$$

For an argon discharge in which T is a few electronvolts and L several tens of centimetres, the gas pressure is on the order of 10 mTorr.

The solutions of the dispersion relation, equations (59), (65) and (56), are reduced at the limit (68) to

$$\begin{gathered}(1)\quad \frac{\beta NL}{2c_s} = \frac{\pi}{2} - 1, \qquad (2)\quad \frac{\beta NL}{2c_s} = \frac{\alpha_G}{b_P^{1/2}}, \\ (3)\quad \frac{\beta NL}{2c_s} = \frac{1}{b_P}\left(\frac{\pi}{2}\right)^2\frac{3c_s}{4v_T}.\end{gathered} \tag{71}$$

Although the relations between the various physical parameters are clearer in equation (71), we find that for the numerical example, it is useful to express all the quantities as a function of the dimensionless Paschen parameter b_P, the parameter b_0 (which we write as $b_0 = \beta/(\sigma_{iN}c_s)$ at the limit (68)), and the ratio v_T/c_s. In this way we show the relation between the Paschen parameter b_P and the electron temperature T and other gas parameters. The dispersion relation in general form and at the three asymptotic limits is

$$\begin{gathered}b_p = \int_0^1 (1-x^2)(b_0 + b_2x^2 + x^3)^{-1}\,dx, \\ (1)\quad b_P = \frac{1}{b_0}\left(\frac{\pi}{2} - 1\right), \qquad (2)\quad b_P^{3/2} = \frac{\alpha_G}{b_0}, \\ (3)\quad b_P^2 = \frac{1}{b_0}\left(\frac{\pi}{2}\right)^2\frac{3c_s}{4v_T}.\end{gathered} \tag{72}$$

The quantity b_2 is $b_2 = b_0 + \frac{4}{3}(v_T/c_s)P((2/\sqrt{\pi})(c_s/v_T)x)$. We now express β as [1]:

$$\beta \equiv \langle\sigma_{ion}v_{edf}\rangle = \sigma_0 v_{te}\left(1 + \frac{2T}{\epsilon_i}\right)\exp\left(-\frac{\epsilon_i}{T}\right), \tag{73}$$

where $v_{te} \equiv (8T/\pi m_e)^{1/2}$ and $\sigma_0 \equiv \pi(e/4\pi\epsilon_0\epsilon_i)^2$, ϵ_0 being the permittivity of the vacuum and ϵ_i the ionization energy. Figures 1–5 show, respectively, T, g_s, $1/\varepsilon_T$, $-\phi_s$ and n_0a^2 as a function of $\log_{10} b_P$ for argon (σ_{iN} is estimated as $\sigma_{iN} = 10^{-18}\,m^2$ [26] and $\epsilon_i = 15.76\,eV$, and the gas is at room temperature, $T_g = 0.026\,eV$). In figure 1 the four relations between the temperature T and b_P are determined by equation (72). The ratio of the plasma densities at the sheath edge and at the centre in the general form (33) and at the three limits, collisionless (58), nonlinear diffusion (64) and linear diffusion (56), is

$$\begin{gathered}g_s = \exp\left\{-\int_0^1 \frac{[(b_0+b_2)x + x^2]}{(b_0 + b_2x^2 + x^3)}\,dx\right\}, \\ (1)\quad g_s = \tfrac{1}{2}, \qquad (2)\quad g_s = \frac{\alpha_G^{1/3}}{b_P^{1/2}}, \\ (3)\quad g_s = \frac{\pi}{2b_p}\left(\frac{3c_s}{4v_T}\right).\end{gathered} \tag{74}$$

These four dependences are shown in figure 2. Figure 3 shows $1/\varepsilon_T$, the particle flux per power unit, as a function of $\log_{10} b_p$. We approximate the energy cost for ionization as $\varepsilon_c = 120\,eV - 20T$, which is a good approximation for $2\,eV \leqslant T \leqslant 4\,eV$. Since ε_T is a nonmonotonic function of T, so is $1/\varepsilon_T$. Figure 4 shows the plasma potential $-\phi_s$ as a function of $\log_{10} b_p$. The plasma potential $-\phi_s$ is determined by equation (19) as $-\phi_s = -(T/e)\ln g_s$, while g_s and T take their accurate values or one of the approximated forms, as specified in equation (74). Note that the plasma potential is also not monotonic with respect to b_p since it is a product of T and $\ln g_s$, which is a decreasing function of T.

In order to calculate the maximal line density n_0a^2 we employ the equation

$$n_0a^2 = \frac{P}{2\pi\bar{f}(gv_z)_{z=L/2}\varepsilon_T}. \tag{75}$$

At the diffusion limit in the radial direction, the radial profile is described by (95) so that $\bar{f} = 0.432$. Figure 5 shows

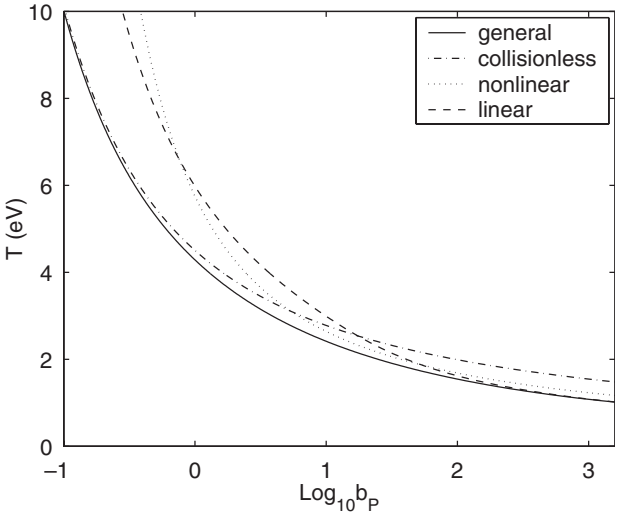

Figure 1. The electron temperature T as a function of $\log_{10} b_P$ for argon. The four relations are determined by equation (72).

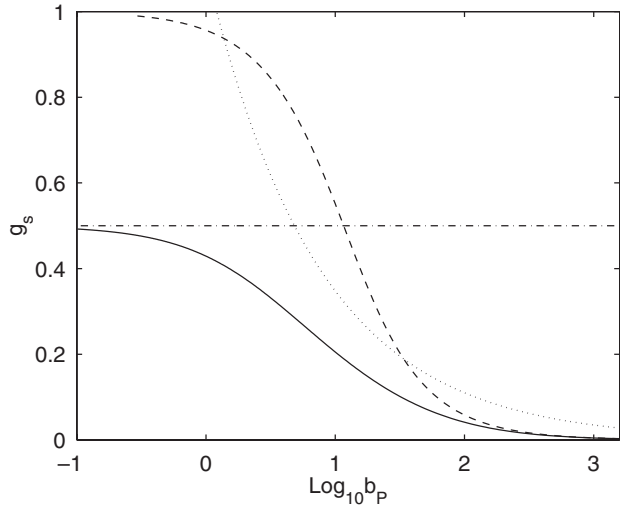

Figure 2. The density ratio g_s as a function of $\log_{10} b_P$ for argon. The four relations are determined by equation (74). The four curves denote the same four cases as in figure 1.

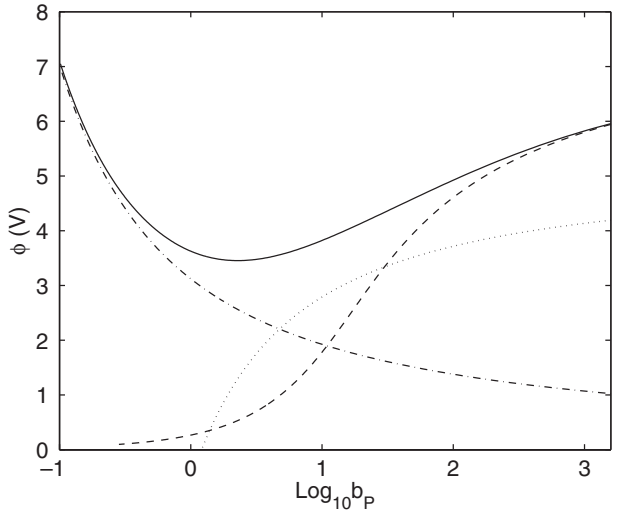

Figure 4. The plasma potential $-\phi_s$ as a function of $\log_{10} b_p$ for argon. The four curves denote the same four cases as in figure 1.

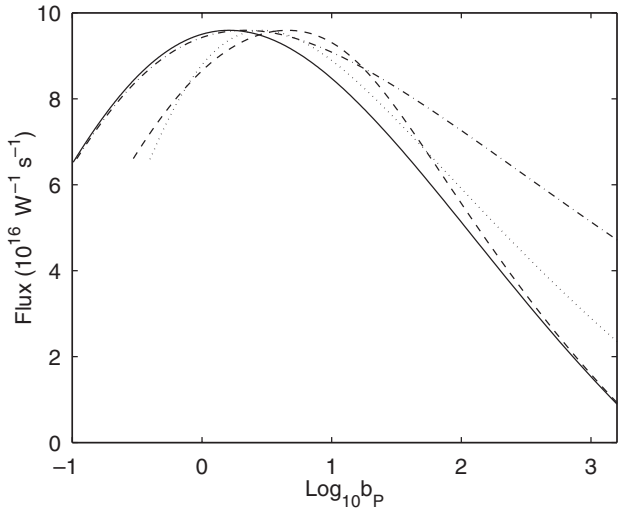

Figure 3. The particle flux per power unit, $1/\varepsilon_T$, as a function of $\log_{10} b_p$ for argon. The four curves denote the same four cases as in figure 1.

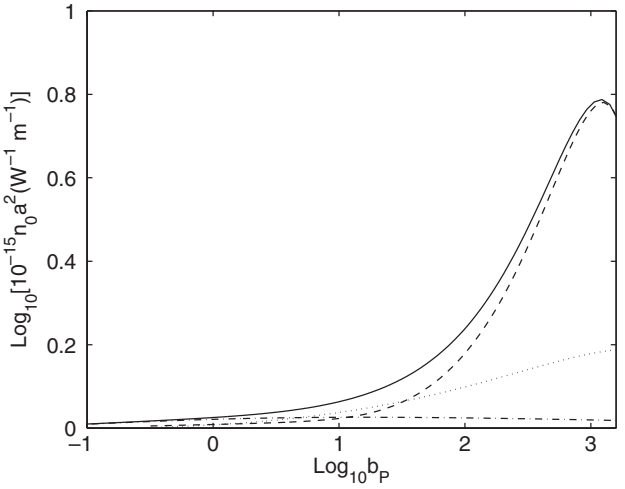

Figure 5. The density per unit length n_0a^2 as a function of $\log_{10} b_p$ for argon. The four curves denote the same four cases as in figure 1.

n_0a^2 as a function of $\log_{10} b_p$, for the general case and for the three approximate cases. For each of the four cases the temperature is determined by the solutions in equation (72), and we use the values of $(gv_z)_{z=L/2} = g_s c_s$, where g_s is given by equation (74). The nonmonotonic behaviour of ε_T is reflected in the nonmonotonic behaviour of n_0a^2.

In the next section we describe the experimental system and experimental results that we compare to our theoretical calculations.

5. The experimental system

The experimental system is shown in figure 6. This is a helicon plasma source that is composed of a vacuum chamber, a gas flow controller, solenoids that generate an axial magnetic field, a radiofrequency generator with matching units and an antenna. The plasma is generated inside a Pyrex tube, 52 cm in length and 10 cm in diameter. The radiofrequency generator radiates at 13.56 MHz and the power is varied in the experiments described here up to 500 W. The antenna is a helix of six turns of a total length of 35 cm and a 11 cm diameter. The wave excited by the antenna and its coupling to the plasma are not discussed in this paper. The magnetic field intensity is varied up to 700 G. The vacuum chamber and Pyrex tube are pumped to a base pressure of 5×10^{-6} Torr. The working gas in the measurements described here is argon. The argon mass flow rate was 7.1 standard cubic centimetres per minute (sccm) and the working pressure 2.5 mTorr.

Employing a Langmuir probe system we have measured the ion saturation current for various wave power levels and magnetic field intensities. The probe was a flat tungsten probe of diameter 1 mm that was protected by a L-filter ($L = 0.46$ mH) and was operated at a potential -100 V referenced to ground. The ion density was calculated from the ion saturation current according to the usual model of

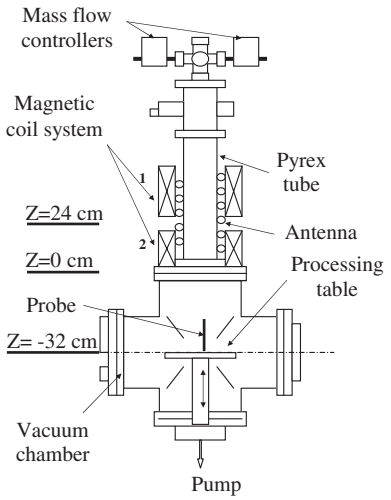

Figure 6. The experimental system.

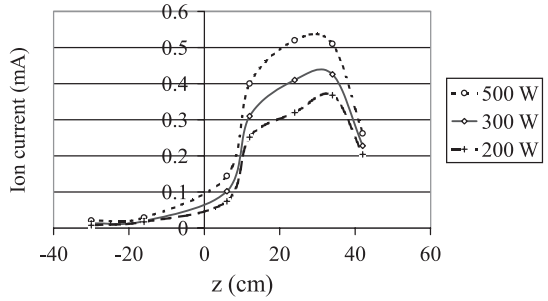

Figure 7. The ion saturation current along the axis of symmetry of the helicon source for three different wave powers. The magnetic field intensity is 650 G. The coordinate z is as shown in figure 6.

a planar probe with a collisionless sheath. This method is applicable as long as the sheath size is much smaller than the probe dimension. For our parameters the plasma density should be much larger than $2 \times 10^{10}\,\mathrm{cm}^{-3}$. The lower density reported here is $2 \times 10^{11}\,\mathrm{cm}^{-3}$, so that the above condition for validity is reasonably satisfied. In the figures the zero of the z axis is located on the connection plane of the Pyrex tube and the vacuum chamber (see figure 6). The antenna is therefore located between $z = 8\,\mathrm{cm}$ and $z = 43\,\mathrm{cm}$. A processing table is positioned in the vacuum chamber at $z = -32\,\mathrm{cm}$.

Figures 7 and 8 present some results of the measurements. Figure 7 shows the ion saturation current at various locations along the axis of symmetry of the Pyrex tube for three different values of wave power at a magnetic field intensity of 650 G. As expected, the density increases when the wave power is increased. However, the density profile is not symmetric in the z direction with respect to the centre of the cylinder, in contradiction to the theortically calculated profiles in section 6. This measured asymmetry probably results from nonuniformities, perhaps in the neutral gas density or in the electron temperature. Despite the difficulty in describing the details of the measured density distribution by the theory, we use the theory to understand the dependence of average values of the plasma density on the magnetic field intensity and on the wave power.

Figure 8 shows the ion saturation current at the centre of the discharge as a function of the magnetic field intensity

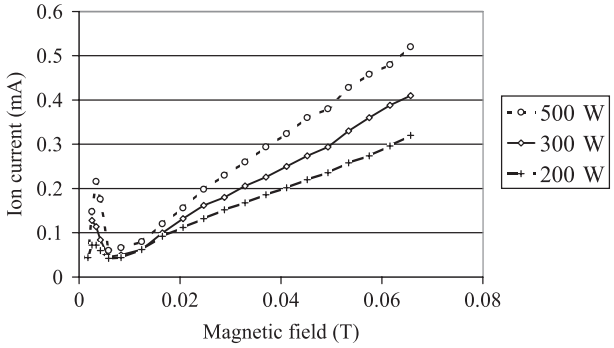

Figure 8. The ion saturation current at the centre of the discharge as a function of the magnetic field intensity for three different values of wave power.

for three different values of the wave power. Apparent are the increase of the ion saturation current and of the deduced plasma density with the increase of both the intensity of the magnetic field and the wave power. A similar increase of the plasma density with the increase of the magnetic field intensity in a helicon source has recently been shown [24]. In that experiment the cylindrical tube is closed at its far end and the length of the source L is well defined. In the analysis of our experiment we also assume that the plasma length is effectively the Pyrex tube length. This assumption is not necessarily accurate for our experiment. In a configuration such as ours, in which the plasma expands from the helicon source into a wide chamber, it can reach supersonic velocities somewhere in the chamber, as has been suggested theoretically [27]. Indeed, recently, an abrupt acceleration to supersonic velocities in a form of a double layer has been discovered [28, 29] and later reconfirmed [30]. We believe, however, that the inaccuracy associated with our assumption has only a small effect on the calculation of the plasma steady state.

The ion saturation current in figure 8 is not monotonic at low values of the magnetic field intensity. Such nonmonotonic behaviour is often observed [31] and has been theoretically addressed [32].

As stated in the introduction, we examine here the suggestion that the reason for the observed increase in density with the increase of the magnetic field intensity is an improved radial confinement by the magnetic field. To that end we solve in the next section the set of equations that describe the radial transport, equations (9)–(11).

6. Radial transport

In our attempt to investigate the effect of the magnetic field intensity on the plasma parameters, we could have made the diffusion approximation for the radial transport. We would then have used the expression for v_r from equation (67). Moreover, assuming that one of the three asymptotic limits for the axial transport is valid, we could have used one of the approximate dispersion relations, equations (106), (108) or (104). Since we want to retain the ion inertia in the radial direction as well as the azimuthal component of the ion velocity, we cannot make the diffusion approximation in the radial direction. We solve the equations for the radial transport in their original, more general form (equations (9)–(11)).

However, rather than solving the full set of equations (9)–(13) that describe the coupled axial and radial dynamics, we make use of the approximate analytical results derived in the previous section for the axial direction. In our experiment the pressure of the argon gas is 2.5 mTorr, and, as before, $\sigma_{iN} = 10^{-18}\,m^2$ [26] and the gas is at room temperature, $T_g = 0.026\,eV$. The calculated Paschen parameter turns out to be $b_p = 18 \gg 1$. Therefore, according to equation (60) the ion inertia can be neglected in the equations that describe the axial transport. For $T = 3\,eV$ and for our plasma length the critical pressure (70) is about 7.5 mTorr, larger than the pressure in our experiment (in [24] the gas pressure is similar but the tube is longer, making the gas pressure and the critical pressure of similar values). This means that in our experiment the right inequality in (66) holds. If also the left inequality in (66) holds, we can assume that the axial dynamics is dominated by nonlinear diffusion. We make this assumption here, reminding the reader that if the form for ν_r in equation (67) is valid, the left inequality in (66) holds for a strong magnetic field. We note that, as is seen in figures 1–5, even when nonlinear diffusion is dominant, retaining nonlinear diffusion only in the calculation leads to a certain inaccuracy. The resulting calculated temperature is probably overestimated by few per cent and the density is underestimated by roughly 30%.

Assuming that the axial dynamics is approximately dominated by nonlinear diffusion, we therefore write the parameter ν_r as

$$\nu_r = \beta N - \frac{2c_s\alpha_G}{Lb_P^{1/2}}, \tag{76}$$

according to equation (65). Equations (9)–(11), in dimensionless form, become

$$\frac{\partial f}{\partial \xi} = \left(\frac{a\beta N}{c_s} - \frac{2\alpha_G a}{L}\sqrt{\frac{2}{\sigma_{iN}NL}}\right)\frac{f}{M_r} - \frac{f}{\xi} - \frac{f}{M_r}\frac{\partial M_r}{\partial \xi}, \tag{77}$$

$$(1 - M_r^2)\frac{\partial M_r}{\partial \xi} = \left(\frac{a\beta N}{c_s} - \frac{2\alpha_G a}{L}\sqrt{\frac{2}{\sigma_{iN}NL}}\right) + \left(\frac{a\nu_{rr}}{c_s} + \frac{a\beta N}{c_s}\right)M_r^2 - \frac{a\nu_{r\theta}}{c_s}M_\theta M_r - \left(1 + M_\theta^2\right)\frac{M_r}{\xi} \tag{78}$$

and

$$M_r\frac{\partial M_\theta}{\partial \xi} = -\left(\frac{a\nu_{\theta\theta}}{c_s} + \frac{a\beta N}{c_s}\right)M_\theta - \frac{a\nu_{\theta r}}{c_s}M_r - \frac{M_\theta M_r}{\xi}. \tag{79}$$

In these equations

$$M_r \equiv \frac{v_r}{c_s}, \qquad M_\theta \equiv \frac{v_\theta}{c_s}, \qquad \xi \equiv \frac{r}{a}. \tag{80}$$

The boundary conditions are a regularity of the solutions at $\xi = 0$ and $M_r(\xi = 1) = 1$. Here, as in our experiment, $a = 5\,cm$, $L = 45\,cm$ and $N = P_g/T_g = 8 \times 10^{19}\,m^{-3}$. In calculating the numerical values of the coefficients in these equations, we use the following expressions for the collision frequencies. The electrons collide with the argon neutrals at a frequency $\nu_{eN} = \langle\sigma_{eN}v_{edf}\rangle N$, where σ_{eN} is the electron–neutral collision cross-section. We use an expression that approximates the values of $\langle\sigma_{eN}v_{edf}\rangle$ as given in the plot in [26]. The electrons are first assumed to collide with ions at the classical binary collision frequency [33] $\nu_{ei} \cong 2.9 \times 10^{-12} n \ln\Lambda T^{-3/2}\,s^{-1}$. In these two expressions the neutral gas and plasma densities are expressed in m^{-3} while T is expressed in electronvolts. The ion–neutral collisions are not important in the plasma radial transport. We therefore do not make a detailed analysis of these collisions, as we did do in section 3. Rather we assume, for simplicity, that the collision operator can be linearized, so that the collision frequency is $\nu_{iN} = \frac{4}{3}\sigma_{iN}v_T N$ as in equation (24). For the specified geometry, gas pressure and magnetic field intensity, the electron temperature turns out, as before, to be an eigenvalue of the problem. The second eigenvalue, ν_r, has been eliminated by employing equation (76). In fact, since ν_{ei} is a function of the plasma density both the electron temperature *and* the electron density are unknowns in equations (9)–(11). Moreover, the electron density is not uniform. We approximate the electron density n in the expression for ν_{ei} by $n_0/2$. The peak density n_0 is calculated from the expression

$$n_0 = \frac{P\alpha_G^{2/3}}{\bar{f}V\beta N\varepsilon_T}, \tag{81}$$

obtained from equations (7), (14) and (22). Here $\bar{f}$ is found by a numerical calculation according to the definition in (20). We also use the relation $\bar{g} = 1/\alpha_G^{2/3}$ from equation (64).

We assume that the wave power that is radiated by the antenna and not reflected towards the generator is completely deposited in the plasma. That value of wave power is substituted as P in equation (81). This assumption will be questioned later.

The values of T and of n_0 as functions of the magnetic field intensity B, calculated for various wave powers P, are shown in figures 9 and 10. The electron temperature T *decreases* when the magnetic field *increases*. We do not present here measurements of T, but such a dependence of T on B has been recently measured [24]. Since the electron temperature T also depends on the electron density n_0 (through the electron collisionality), which, in turn, depends on the wave power P (equation (81)), the electron temperature in figure 9 also depends on the wave power. However, as seen in the figure, the differences between the values of T for different values of wave power P are small. The dependence is weak because electrons collide with ions much less than with neutrals, and therefore the dependence of the total electron collisionality on the ion density is also small.

As seen in figure 10, the measured dependence of the plasma density n_0 on the magnetic field intensity and on the wave power is qualitatively similar to the dependence predicted by the solution of the equations. The density increases as either B or P are increased. However, in contrast to the qualitative similarity between the experimental and theoretical dependencies, there is a striking quantitative disagreement. The density calculated from the measurements is significantly lower than the density found by a solution of the equations. Moreover, while the the calculated density reaches saturation around a magnetic field somewhat larger than 100 G, the measured density keeps increasing even at the maximal magnetic field of 650 G, albeit with values lower than the

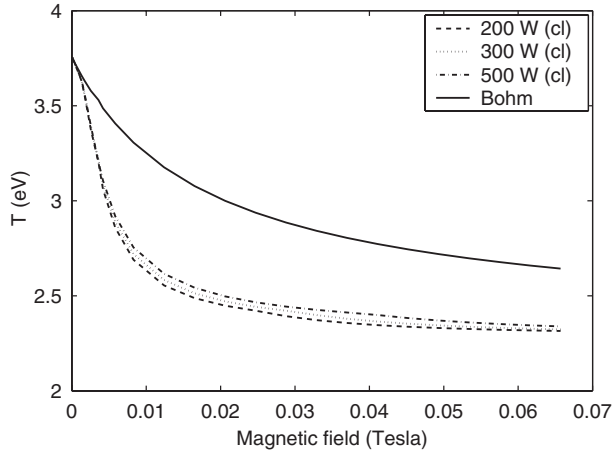

Figure 9. The electron temperature as a function of the magnetic field intensity. The three dotted lines show the results for a classical electron collisionality. The solid line is for the case of anomalous Bohm electron collisionality.

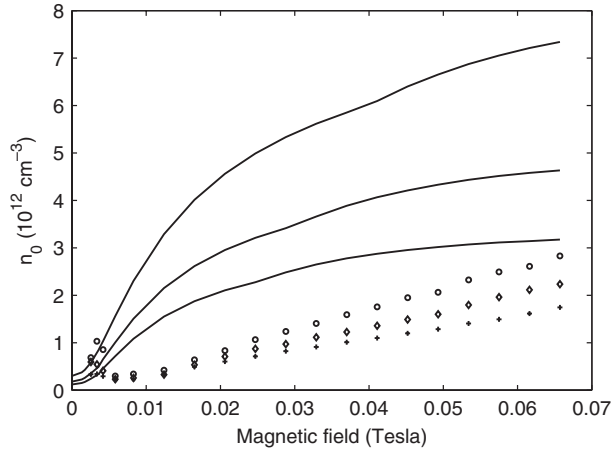

Figure 10. The measured (discrete signs) and calculated (——) density n_0 as a function of the magnetic field intensity for the three wave powers as in figure 9. The density is calculated with the assumption of classical electron collisionality.

calculated ones. The value of the magnetic field at saturation can be estimated from equation (108),

$$\frac{\beta N L}{2c_s} = \frac{p_1^2}{2a^2}\frac{c_s \nu_e L}{\omega_{ci}\omega_{ce}} + \frac{\alpha_G}{b_P^{1/2}}. \tag{82}$$

The two terms on the RHS of the equation represent plasma radial and axial transport. The rate of the radial transport is determined mostly by electron cross-field diffusion that is induced by electron collisions across the impeding magnetic field. The origin of the increase of the density n_0 with the increase of magnetic field intensity B for a fixed value of wave power P could be the improved radial confinement by the magnetic field. That improved confinement results from the radial electron mobility being impeded by the magnetic field, as expressed by the term $\omega_{ci}\omega_{ce}/\nu_e$ in the coefficient ν_{rr}, and in the approximated dispersion relation (108). The plasma axial transport is determined by the ion mobility that is impeded, in our case, by nonlinear collisions with neutrals, and is not affected by the magnetic field intensity. When the magnetic field is strong enough the radial transport becomes much smaller than the axial transport and the density does not continue to increase as the magnetic field increases. This should happen when

$$\frac{p_1^2}{2a^2}\frac{c_s \nu_e L}{\omega_{ci}\omega_{ce}} \ll \frac{\alpha_G}{b_P^{1/2}}. \tag{83}$$

If $c_s \simeq 2460\,\mathrm{m\,s^{-1}}$ and $\nu_e \approx 10^7\,\mathrm{s^{-1}}$ ($T \approx 3\,\mathrm{eV}$), then $B \gg 100\,\mathrm{G}$ for inequality (83) to hold. This estimate of the magnetic field intensity at which the plasma density saturates, indeed agrees with the full numerical solution but contradicts the experimental result, both are shown in figure 10.

Nevertheless, we can interpret the increase of density with the increase of magnetic field intensity as a result of improved confinement only if we assume an electron collision frequency ν_e that is higher than the sum of electron–neutral and electron–ion collision frequencies, as was used in the calculations shown in figure 10. We choose a value that corresponds to Bohm diffusion,

$$\nu_e = \frac{\omega_{ce}}{16}. \tag{84}$$

As is shown in figure 11, the plasma density that is calculated with this value for the electron collisionality agrees with the measurements. The dependence of T on B in the case that equation (84) holds is also shown in figure 9. The decrease of T is much slower in this case.

Further support for the interpretation of the density increase with the increase of the magnetic field intensity as a result of an improved radial confinement, might be found in figures 12–14. Figures 12 and 13 show the calculated normalized plasma flow velocity and density. In figure 12 the plasma is not magnetized. There is no plasma rotation and the radial velocity increases gradually towards the wall. The radial profile is relatively flat and the plasma density near the wall is quite high relative to the peak plasma density. This means that a large part of the plasma is lost radially. Figure 13 presents the opposite case of a strongly magnetized plasma (0.13 T in the calculation, but it is similar at 0.08 T, the maximal magnetic field in the experiment). In the magnetized plasma the density is peaked at the cylinder axis, and there is a small region only near the radial wall in which the plasma is accelerated to the sonic velocity. The density at the wall is very small (and so is the radial flux to the wall). Interestingly, there is a small plasma rotation—the velocity M_θ is not zero. Such a rotation is possible in a magnetized plasma if there are electon–neutral collisions, as is clear from equation (79). Figure 14 shows the radial profile of the density at the axial centre of the plasma as calculated from the probe measurements. Indeed, as the magnetic field is increased, the ratio of the plasma densities at the edge and on axis becomes smaller, similarly to the ratio that could be calculated from the theoretical results shown in figures 12 and 13. The anomalously high collisionality is therefore consistent with the dependence of the radial plasma-density profile on the magnetic field intensity, as we see experimentally. It is also consistent with the weak dependence of the plasma impedance on the magnetic field intensity that we indeed observe.

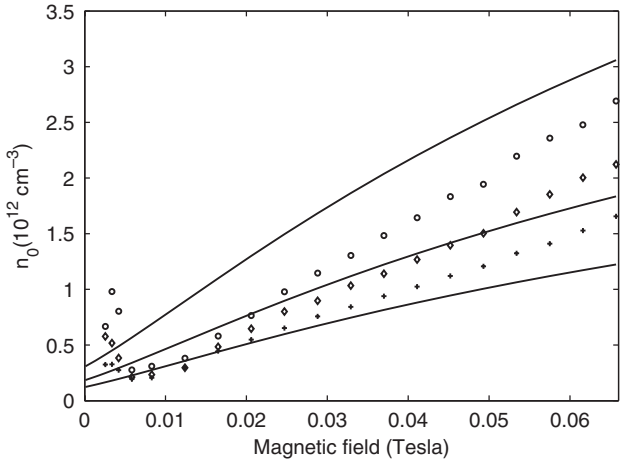

Figure 11. The measured (signs) and calculated (——) density n_0 as a function of the magnetic field intensity for the three values of wave power as in figure 9. The density is calculated with the assumption of anomalous Bohm electron collisionality.

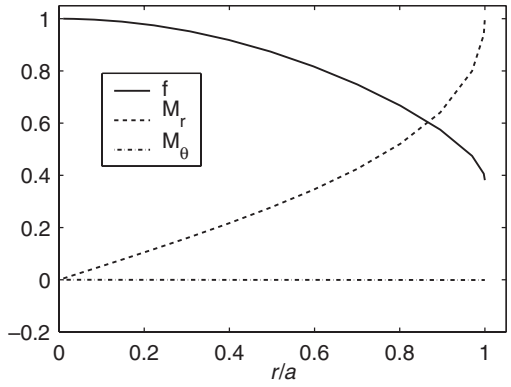

Figure 12. The calculated normalized plasma flow velocity and density as a function of r in a nonmagnetized plasma. There is no plasma rotation and the radial velocity increases gradually towards the wall. The radial profile is relatively flat and the plasma density near the wall is quite high relative to the peak plasma density. A large part of the plasma is lost radially.

Despite this seemingly ample evidence for the anomalous electron collisions, we find it hard to conclude that such a high anomalous electron collisionality actually exists in our plasma (at $B = 600$ G the collision frequency according to equation (84) should be about 60 times the classical collisionality). We cannot point to any mechanism that could cause such a high anomalous collisionality. We suggest, rather, a second process that should be examined as the main reason for the density increase. This second process is an improved wave–plasma coupling via the helicon interaction, causing a larger fraction of the total wave power to actually be deposited inside the helicon source. The power P that should be employed in equation (81) is not the power radiated by the antenna, but rather that fraction of the power actually deposited in the plasma, a fraction that increases with the increase of the magnetic field. The fate of the power that is not absorbed in the plasma, whether it is absorbed in a sheath near the antenna, in the dilute plasma in the vacuum chamber, or elsewhere, will be investigated in the future.

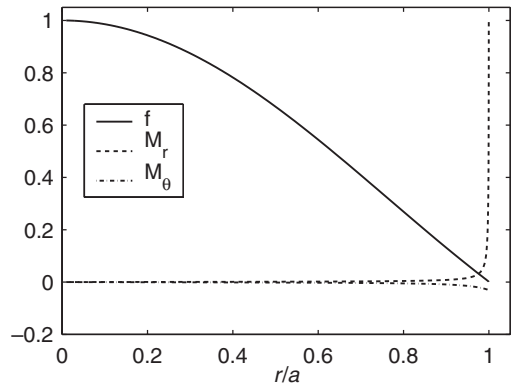

Figure 13. The calculated normalized plasma flow velocity and density as a function of r in a magnetized plasma (0.13 T). The density is peaked at the cylinder axis, and there is a small region only, near the radial wall, in which the plasma is accelerated to the sonic velocity. The density at the wall is very small (and so is the radial flux to the wall). There is a small plasma rotation.

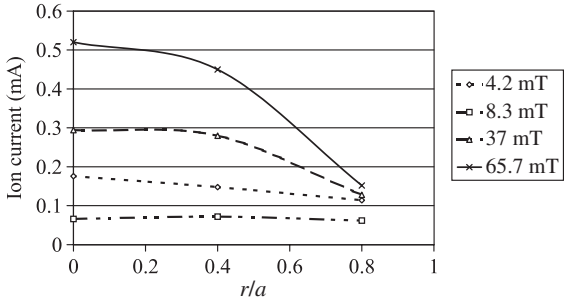

Figure 14. The radial profile of the density at the axial centre of the plasma as calculated from the probe measurements. As the magnetic field is increased, the ratio of the plasma densities at the edge and on axis becomes smaller, similarly to that shown in figures 12 and 13.

7. Summary

We have developed a two-dimensional steady-state model, in which, even though ion inertia was retained, a variable separation enabled us to analyse separately the axial and the radial transports. For the axial transport (along magnetic field lines) an integral dispersion relation was derived that includes a nonlinear form obtained from the ion–neutral collision operator, in which the neutrals have a finite temperature. The dispersion relation was solved for various values of the Paschen parameter and was shown to have three asymptotic limits: collisionless, linear diffusion and nonlinear diffusion. The results obtained by solutions of the model equations, that include the impeding of the radial transport by the magnetic field, were compared to probe measurements performed inside our helicon source. We have shown that the proposition that the measured increase in the plasma density with the increase of the magnetic field intensity is a result of an improving confinement, implies that the electron collisionality is much larger than expected from electron–ion and electron–neutral collisions. When Bohm diffusion was assumed, a good agreement between theory and experiment was found.

Since the collisionality that could cause Bohm diffusion is anomalously high in our case, we suggest a different explanation for the dependence of the density on the magnetic field intensity. This different explanation, that the density

increase that follows an increase of the magnetic field intensity results from an improved wave–plasma coupling via the helicon interaction, will be examined in the future. The assumption that the neutral density does not vary will also be relaxed and neutral depletion will be incorporated in the model.

We believe that the analysis presented here is a significant step towards a more comprehensive analysis, that should address simultaneously the wave energy deposition in the plasma and the transport processes. Such an analysis should also provide the spatial distribution of the electron temperature by including an energy equation for the electrons.

Acknowledgments

The authors benefited from discussions with Professors R W Boswell, N Hershkowitz, M A Lieberman, F F Chen, S Shinohara, V A Godyak and B N Breizman. This research was supported by the Israel Science Foundation (grant no. 59/99) and by the Quarter Micron Consortium.

Appendix A. The collision term

Here we derive the form of the transport coefficient $\nu_{zz} = \nu_{iN} + (m_e/m_i)\nu_{eN} \cong \nu_{iN}$. To that end we calculate the drag on the ions due to their collisions with neutrals. We start by writing the Boltzmann collision operator [34]

$$\frac{\partial f(\vec{v}_i)}{\partial t} = \int \mathrm{d}\vec{v}_N \int \mathrm{d}\Omega \frac{\mathrm{d}\sigma}{\mathrm{d}\Omega}|\vec{v}_i - \vec{v}_N| \times [F_i(\vec{v}_i')F_N(\vec{v}_N') - F_i(\vec{v}_i)F_N(\vec{v}_N)] \tag{85}$$

for charge-exchange and elastic ion–neutral collisions. For the ion energies we are interested in, the cross-sections for both types of collisions are approximately constant. Also, the total ion and neutral momenta is conserved, $\vec{v}_N' = \vec{v}_i + \vec{v}_N - \vec{v}_i'$. We therefore write

$$\mathrm{d}\Omega \frac{\mathrm{d}\sigma_{cx}(\vec{v}_i, \vec{v}_N, \vec{v}_i', \vec{v}_N')}{\mathrm{d}\Omega} = \mathrm{d}\vec{v}_i' \sigma_{cx} \delta(\vec{v}_i' - \vec{v}_N),$$
$$\mathrm{d}\Omega \frac{\mathrm{d}\sigma_{el}}{\mathrm{d}\Omega} = \frac{\sigma_{el}}{2\pi} v_{i,cm}' \, \mathrm{d}v_{i,cm}' \delta(v_{i,cm}'^2 - v_{i,cm}^2) \, \mathrm{d}(\cos\theta_{cm}') \, \mathrm{d}\varphi_{cm}'. \tag{86}$$

Here, for the elastic collisions the cross section is isotropic at the centre-of-mass frame of reference, the velocity of which is $\vec{v}_{CM} = (\vec{v}_i + \vec{v}_N)/2$. The angle θ_{cm} is measured at the centre-of-mass frame of reference with respect to $v_{i,cm}$. Integrating over $\vec{v}_i'$ yields

$$\frac{\partial f(\vec{v}_i)}{\partial t_{cx}} = \sigma_{cx} \int \mathrm{d}\vec{v}_N |\vec{v}_i - \vec{v}_N| [F_i(\vec{v}_N)F_N(\vec{v}_i) - F_i(\vec{v}_i)F_N(\vec{v}_N)] \tag{87}$$

for charge-exchange collisions and

$$\frac{\partial f}{\partial t_{el}} = \sigma_{el} \int \mathrm{d}\vec{v}_N \Bigg[\int \frac{v_{i,cm}'^2}{\pi} \mathrm{d}v_{i,cm}' \delta(v_{i,cm}'^2 - v_{i,cm}^2) \, \mathrm{d}(\cos\theta_{cm}') \times \mathrm{d}\varphi_{cm}' F_i(\vec{v}_i')F_N(\vec{v}_N') - F_i(\vec{v}_i)|\vec{v}_i - \vec{v}_N|F_N(\vec{v}_N) \Bigg] \tag{88}$$

for elastic collisions. In the expression for the elastic collisions we used the relation $|\vec{v}_i - \vec{v}_N| = 2v_{i,cm}'$.

We now make the assumption that the ion and neutral distributions are known. In particular, we neglect the ion pressure, as we did in the previous sections. Also, we assume that the neutral distribution is Maxwellian. Therefore,

$$F_i(\vec{v}_i) = n\delta(\vec{v}_i - \vec{v}),$$
$$F_N(\vec{v}_N) = N \left(\frac{m_i}{2\pi T_g}\right)^{3/2} \exp\left(-\frac{m_i v_N^2}{2T_g}\right). \tag{89}$$

For the charge-exchange collisions, the collision operator takes the form

$$\frac{\partial f(\vec{v}_i)}{\partial t_{cx}} = Nn\sigma_{cx} \left(\frac{m_i}{2T_g}\right) \left\{ |\vec{d}_i - \vec{d}| \frac{\exp(-d_i^2)}{\pi^{3/2}} - \delta(\vec{d}_i - \vec{d}) \left[\frac{\exp(-d_i^2)}{\sqrt{\pi}} + \left(d_i + \frac{1}{2d_i}\right) \mathrm{erf}(d_i) \right] \right\}. \tag{90}$$

In these expressions

$$\vec{d}_i \equiv \left(\frac{m_i}{2T_g}\right)^{1/2} \vec{v}_i, \qquad \vec{d} \equiv \left(\frac{m_i}{2T_g}\right)^{1/2} \vec{v} \tag{91}$$

and erf denotes the error function. In order to perform the integration in equation (88) we write the ion distribution function in spherical coordinates as $F_i(\vec{v}_i) = (2n/v_i)\delta(v_i^2 - v^2)\delta(\cos\theta_i - \cos\theta)\delta(\varphi_i - \varphi)$. After integrating over $\vec{v}_i'$ we employ the relation $\delta(v_{cm}^2 - v_{i,cm}^2) = \delta[(\vec{v}_i - \vec{v}) \cdot (\vec{v}_N - \vec{v})]$ for integration over $\vec{v}_N$. The integration is then performed over $(\vec{v}_N - \vec{v})_\perp \equiv (\vec{v}_N - \vec{v}) - (\vec{v}_N - \vec{v}) \cdot (\vec{v}_i - \vec{v})(\vec{v}_i - \vec{v})/|\vec{v}_i - \vec{v}|^2$, resulting in

$$\frac{\partial f}{\partial t_{el}} = Nn\sigma_{el} \left(\frac{m_i}{2T_g}\right) \left\{ \frac{\exp[-(\vec{d}_i \cdot (\vec{d}_i - \vec{d})/|\vec{d}_i - \vec{d}|)^2]}{|\vec{d}_i - \vec{d}|\pi^{3/2}} - \delta(\vec{d}_i - \vec{d}) \left[\frac{\exp(-d_i^2)}{\sqrt{\pi}} + \left(d_i + \frac{1}{2d_i}\right) \mathrm{erf}(d_i) \right] \right\}. \tag{92}$$

The drag is found by calculating $\int \mathrm{d}\vec{v}_i m_i \vec{v}_i \partial f(\vec{v}_i)/\partial t$, which, as a result of conservation of the number of particles, equals $\int \mathrm{d}\vec{v}_i m_i (\vec{v}_i - \vec{v}) \partial f(\vec{v}_i)/\partial t$. The drag for charge exchange collisions is of the form $m_i n \sigma_{cx} \int \mathrm{d}\vec{v}_N |\vec{v}_N - \vec{v}| (\vec{v}_N - \vec{v}) F_N(\vec{v}_N)$. For the specific distribution functions we chose, for the case of no ion pressure, the integrals over the second terms in the collision operators in equations (92) and (90) vanish, and the total drag becomes

$$\vec{F} = -m_i \vec{v} \left(\frac{2T_g}{m_i}\right)^{1/2} Nn\sigma_{iN} \left[\left(d + \frac{1}{d} - \frac{1}{4d^3}\right) \mathrm{erf}(d) + \frac{1}{\sqrt{\pi}} \left(1 + \frac{1}{2d^2}\right) \exp(-d^2) \right],$$
$$\sigma_{iN} \equiv \sigma_{cx} + \frac{\sigma_{el}}{2}. \tag{93}$$

Appendix B. The diffusion regime

We make the approximations of neglecting the ion inertia in both axial and radial directions as well as the azimuthal ion velocity, so that $v_\theta = 0$. The equations that govern the ion radial transport [(9) and (10)], in which we neglect the LHS,

become

$$\frac{c_s^2}{\nu_{rr}}\frac{\partial}{\partial r}\left(r\frac{\partial}{\partial r}f\right)+\nu_r r f=0,$$
$$-c_s^2\left(\nu_r-\frac{\partial}{\partial r}v_r-\frac{v_r}{r}\right)-\nu_{rr}v_r^2=0. \tag{94}$$

Requiring that $f(r=a)=0$ (and equivalently $v_r(r=a)=\infty$), we obtain the solution of these diffusion equations as

$$f(r)=J_0\left(\frac{p_1 r}{a}\right),\qquad v_r(r)=\frac{p_1}{a}\frac{c_s^2}{\nu_{rr}}\frac{J_1(p_1 r/a)}{J_0(p_1 r/a)},$$
$$\nu_r=\frac{p_1^2}{a^2}\frac{c_s^2}{\nu_{rr}},\qquad \bar{f}=\frac{2}{p_1}J_1(p_1)=0.432. \tag{95}$$

Here J_0 and J_1 are the zero-order and first-order Bessel functions and $p_1=2.4048$ is the first zero of the Bessel function J_0. A solution of the dynamics in the z direction will provide us with an additional relation between ν_r and T. Often we can approximate

$$\nu_{rr}=\frac{\omega_{ci}\omega_{ce}}{\nu_e}. \tag{96}$$

Turning to the axial transport, we combine the continuity equation, equation (31), and equation (25). In equation (25) we neglect the ion inertia, the second term on the LHS (we retain one term due to the ion inertia in order for the calculation here to be consistent with the calculation in section 3). Combining the two equations we obtain the following equation:

$$\frac{\partial}{\partial\zeta}\left[g\left(-1+\sqrt{1-\frac{4}{b_P(b_2)^2 g}\frac{\partial g}{\partial\zeta}}\right)\right]=\frac{2b_P b_0}{b_2}g. \tag{97}$$

The linear and nonlinear diffusions are recovered at the two opposite limits. One is

$$\frac{4}{b_P(b_2)^2}\ll 1\implies \frac{\partial^2 g}{\partial\zeta^2}+b_P^2 b_0 b_2 g=0, \tag{98}$$

which is the linear diffusion, in which:

$$g=\cos(b_P\sqrt{b_0 b_2}\zeta),\quad b_P^2 b_0 b_2=\left(\frac{\pi}{2}\right)^2. \tag{99}$$

The inequality in equation (98) becomes $b_0^{1/3}\ll b_2$ when equation (99) is used to express b_P. At the opposite limit

$$\frac{4}{b_P(b_2)^2}\gg 1,\qquad \frac{\partial}{\partial\zeta}\sqrt{-g\frac{\partial g}{\partial\zeta}}=b_P^{3/2}b_0 g, \tag{100}$$

which is the nonlinear diffusion equation derived by Godyak [2]. Here it is generalized to be coupled with the radial dynamics through the coefficient b_0. The solution of equation (100) is

$$b_P b_0^{2/3}(1-\zeta)=\int_0^g\frac{x\,\mathrm{d}x}{(1-x^3)^{2/3}},$$
$$b_P b_0^{2/3}=\alpha_G^{2/3}=\int_0^1\frac{x\,\mathrm{d}x}{(1-x^3)^{2/3}}. \tag{101}$$

This dispersion relation (the second equality in equation (101)) is equivalent to the dispersion relation derived in section 3 (64). The inequality in equation (100) becomes $b_0^{1/3}\gg b_2$ when equation (101) is used to express b_P. We note that the nonlinear diffusion equation was solved in [4] for the important case of nonuniform gas density, exhibiting the resulting asymmetric plasma density.

Appendix C. Summary of asymptotic results

In this section we summarize the asymptotic limits that were derived in section 3 and in appendix B. Using the expressions for ν_r and for ν_{rr} as given in equation (95) and in equation (96), which are valid in the diffusion approximation in the radial direction for a large enough magnetic field, we write

$$\frac{\nu_r L}{2c_s}=\frac{p_1^2}{2a^2}\frac{c_s\nu_e L}{\omega_{ci}\omega_{ce}}. \tag{102}$$

We substitute this expression for ν_r into the asymptotic expressions for the axial transport derived in section 4 and present here the resulting forms of the various dispersion relations and flow variables.

The linear diffusion limit was described in section 3.2. With the expression (102) the condition (55) for the validity of the linear diffusion approximation becomes

$$\frac{p_1^2}{2a^2}\frac{c_s\nu_e L}{\omega_{ci}\omega_{ce}}+\frac{4\nu_T}{3c_s}b_p\gg\frac{\pi}{2},\quad\sqrt{\frac{\pi}{2}b_P}. \tag{103}$$

The solution of the dispersion relation and the density ratio (56) then become

$$\frac{\beta N L}{2c_s}=\frac{p_1^2}{2a^2}\frac{c_s\nu_e L}{\omega_{ci}\omega_{ce}}+\left(\frac{\pi}{2}\right)^2\left(\frac{p_1^2}{2a^2}\frac{c_s\nu_e L}{\omega_{ci}\omega_{ce}}+\frac{4\nu_T}{3c_s}b_p\right)^{-1},$$
$$g_s=\frac{\pi}{2}\left(\frac{p_1^2}{2a^2}\frac{c_s\nu_e L}{\omega_{ci}\omega_{ce}}+\frac{4\nu_T}{3c_s}b_p\right)^{-1}. \tag{104}$$

As described above, ionization is balanced by radial diffusion and by axial linear diffusion.

The case that the ion inertia should be retained was described in section 3.3. The condition for the validity of this limit (60) is

$$\frac{\pi}{2}-1\gg\frac{p_1^2}{2a^2}\frac{c_s\nu_e L}{\omega_{ci}\omega_{ce}},\qquad 1\gg b_p. \tag{105}$$

The solution of the dispersion relation and the flow variables (58) are

$$\frac{\beta N L}{2c_s}=\frac{\pi}{2}-1,\qquad\left(\frac{\pi}{2}-1\right)\zeta=-M_z+2\arctan(M_z),$$
$$g=\frac{1}{1+M_z^2},\qquad g_s=\frac{1}{2},\qquad \bar{g}\cong\frac{0.5}{\pi/2-1}=0.875\,97. \tag{106}$$

The third case, that of nonlinear diffusion, holds when (66)

$$\left(\frac{p_1^2}{2a^2}\frac{c_s\nu_e L}{\omega_{ci}\omega_{ce}}\right)^2\frac{1}{\alpha_G^{2/3}},\quad\alpha_G^{2/3}\ll b_P\ll\frac{4\alpha_G^{2/3}}{\pi}\left(\frac{c_s}{v_T}\right)^2. \tag{107}$$

The solution of the dispersion relation (65) and the density (64) then become

$$\frac{\beta N L}{2c_s} = \frac{p_1^2}{2a^2}\frac{c_s \nu_e L}{\omega_{ci}\omega_{ce}} + \frac{\alpha_G}{b_P^{1/2}}, \qquad g_s = \frac{\alpha_G^{1/3}}{b_P^{1/2}}, \qquad \bar{g} = \frac{1}{\alpha_G^{2/3}}. \tag{108}$$

As described above, ionization is balanced by radial diffusion and nonlinear axial diffusion.

Examining the three limits, we note that for b_P small, the ion inertia limit holds, while for either a large b_P or a strong radial transport, linear diffusion dominates. At intermediate values of b_P nonlinear diffusion is valid.

References

[1] Lieberman M A and Lichtenberg A J 1994 *Principles of Plasma Discharges and Materials Processing* (New York: Wiley)

[2] Godyak V A 1986 *Soviet Radio Frequency Discharge Research* (Falls Church, VA: Delphic Associates)
Lieberman M A and Lichtenberg A J 1994 *Principles of Plasma Discharges and Materials Processing* (New York: Wiley) p 138

[3] Godyak V A 1990 Non-local bounded plasma model with charge exchange collisions, ESCAMPIG90 *10th European Section Conf. on the Atomic and Molecular Physics of Ionized Gases (Orleans, France, 1990)* ed B Dubreud (European Physics Section)

[4] Breizman B N and Arefiev A V 2002 *Phys. Plasmas* **9** 1015

[5] Gilland J, Breun R and Hershkowitz N 1998 *Plasma Sources Sci. Technol.* **7** 416

[6] Yun S, Taylor K and Tynan G R 2000 *Phys. Plasmas* **7** 3448

[7] Shamrai K P and Taranov V B 1995 *Phys. Lett.* A **204** 139

[8] Arnush D and Chen FF 1998 *Phys. Plasmas* **5** 1239

[9] Lieberman M A and Boswell R W 1998 *J. Phys. IV (France)* **8** 145

[10] Shinohara S and Yonekura K 2000 *Plasma Phys. Control. Fusion* **42** 41

[11] Enk Th and Kramer M 2000 *Phys. Plasmas* **7** 4308

[12] Breizman B N and Arefiev A V 2000 *Phys. Rev. Lett.* **84** 3863

[13] Margot J, Vidal F, Chaker M, Johnston T W, Aliouchouche A, Tabbal M, Delprat S, Pauna O and Benhabib D 2001 *Plasma Sources Sci. Technol.* **10** 556

[14] Cho S and Lieberman M A 2003 *Phys. Plasmas* **10** 882

[15] Kinder R L, Ellingboe A R and Kushner M J 2003 *Plasma Sources Sci. Technol.* **12** 561

[16] Boswell R W 1970 *Phys. Lett.* A **33** 457

[17] Boswell R W and Chen F F 1997 *IEEE Trans. Plasma Sci.* **25** 1229

[18] Chen F F and Boswell R W 1997 *IEEE Trans. Plasma Sci.* **25** 1245

[19] Blackwell D D and Chen F F 1997 *Plasma Sources Sci. Technol.* **6** 569

[20] Chen R T S and Hershkowitz N 1998 *Phys. Rev. Lett.* **80** 3400

[21] Shinohara S and Shamrai K P 2000 *Plasma Phys. Control. Fusion* **42** 865

[22] Carter M D, Baity F W Jr, Barber G C, Goulding R H, Mori Y, Sparks D O, White K F, Jaeger E F, Chang-Diaz F R and Squire J P 2002 *Phys. Plasmas* **9** 5097

[23] Franck C M, Grulke O and Klinger T 2003 *Phys. Plasmas* **10** 323

[24] Tysk S M, Denning C M, Scharer J E and Akhtar K 2004 *Phys. Plasmas* **11** 878

[25] Self S A and Ewald H N 1966 *Phys. Fluids* **9** 2486

[26] Lieberman M A and Lichtenberg A J 1994 *Principles of Plasma Discharges and Materials Processing* (New York: Wiley) p 80

[27] Manheimer W M and Fernsler R F 2001 *IEEE Trans. Plasma Sci.* **29** 75

[28] Charles C and Boswell R 2003 *Appl. Phys. Lett.* **82** 1356

[29] Cohen S A, Siefert N S, Stange S, Boivin R F, Scime E E and Levinton F M 2003 *Phys. Plasmas* **10** 2593

[30] Sun X, Biloiu C, Hardin R and Scime E E 2004 *Plasma Sources Sci. Technol.* **13** 359

[31] Cheetham A D and Rayner J P 1998 *J. Vac. Sci. Technol.* A **16** 2777

[32] Chen F F 2003 *Phys. Plasmas* **10** 2586

[33] Braginskii S I 1965 Transport processes in a plasma *Rev. Plasma Phys.* **1** 250

[34] Krall N and Trivelpiece A 1973 *Principles of Plasma Physics* (New York: McGraw-Hill)